Table 1 Ratios of the maximized fundamental frequencies and optimal location and fiber orientation angle of the bonded sheet: $\alpha = 1$ and $\delta_x = \delta_y = 0.5$

BC	Ω_{max}/Ω_{al}	$(X, Y)_{max}$	θ_{max}, deg	Ω_{min}/Ω_{al}
FFFC	1.261	(0, 0.5)	90	0.970
FFSS	1.091	(0.5, 0.5)	135	0.946
FFSC	1.204	(−0.5, 0.5)	82	0.951
FFCC	1.162	(0.5, −0.5)	15	0.954
FSFC	1.098	(0, 0)	90	0.984
FSSS	1.187	(−0.5, 0)	90	0.976
FSSC	1.135	(−0.5, 0)	92	0.973
FSCS	1.137	(−0.5, 0)	90	0.948
FSCC	1.131	(−0.5, 0.5)	87	0.969
FCFC	1.087	(0, 0.5)	90	0.980
FCSC	1.138	(−0.5, 0.5)	90	0.969
FCCC	1.140	(−0.5, 0.5)	90	0.966
SSSS	1.071	(−0.5, 0.5)	45	1.021
SSSC	1.077	(0, 0.5)	90	1.012
SSCC	1.071	(−0.5, −0.5)	135	1.019
SCSC	1.093	(0, 0.5)	90	1.009
SCCC	1.077	(0, 0.5)	90	1.016
CCCC	1.062	(−0.5, 0)	0	1.026

not virtually affected by the change of angle θ. In contrast, a plate with the sheet at root edge 2, $(X, Y) = (0, 0.5)$, gives the highest frequency because the fundamental mode is a simple bending motion with no nodal line, and it is effective to increase the stiffness at the clamped edge in the bending direction ($\theta = 90$). The difference between the maximum and minimum values in Fig. 3 is more than 25%.

Next the fundamental frequencies of the square plate are calculated for 18 different combinations of classical boundary conditions, that is, F, S, and C. There are 21 different combinations of the classical BCs for an isotropic square plate,[7] but the three cases (FFFF, SFFF, and FSFF) involving rigid-body motions are omitted. The optimal fiber orientation angles θ_{max} are searched to give the maximum fundamental frequencies Ω_{max} for nine given sheet locations in Fig. 2, and the frequency ratios Ω_{max}/Ω_{al} ($\Omega_{max} = \text{maximum}\Omega_1$) are tabulated in Table 1. The ratios of the minimum frequency Ω_{min}/Ω_{al} ($\Omega_{min} = \text{minimum}\Omega_1$) are also given at the rightmost column in Table 1.

IV. Summary

Generally, the sets of BCs are listed in the order of increasing edge constraints, starting from FFFC to CCCC, in Table 1. Note that the ratio Ω_{max}/Ω_{al} is higher (the sheet has more stiffening effect) as more free edges are involved. At the same time, however, there exist ratios Ω_{min}/Ω_{al} that are less than one for BCs including at least one free edge. This means that the location of the bonded sheet has a significant effect for plates with more free edges. In contrast, plates strongly constrained along edges (from SSSS to CCCC) are not significantly influenced by addition of bonded composite sheets.

References

[1]Hollaway, L. C., and Leeming, M. B., *Strengthening of Reinforced Concrete Structures: Using Externally-Bonded Frp Composites in Structural and Civil Engineering*, CRC Press, Boca Raton, FL, 1999.

[2]"Inauguration of Nippon Steel Composite," *Nippon Steel News*, No. 274, May/June 1999.

[3]Irie, T., Yamada, G., and Ikai, H., "Natural Frequencies of Stepped Thickness Rectangular Plate," *International Journal of Mechanical Science*, Vol. 22, 1980, pp. 767–777.

[4]Jones, R. M., *Mechanics of Composite Materials*, 2nd ed., Taylor and Francis, Philadelphia, 1999, pp. 190–202.

[5]Narita, Y., Ohta, Y., Yamada, G., and Kobayashi, Y., "Analytical Method for Vibration of Angle-Ply Cylindrical Shells Having Arbitrary Edges," *AIAA Journal*, Vol. 30, No. 3, 1992, pp. 790–796.

[6]Tsai, S. W., *Composite Design*, 4th ed., Think Composites, Dayton, OH, 1998, B-2.

[7]Narita, Y., "Combinations for the Free-Vibration Behaviors of Anisotropic Rectangular Plates Under General Edge Conditions," *Journal of Applied Mechanics*, Vol. 67, 2000, pp. 568–573.

K. N. Shivakumar
Associate Editor

Experimental Nonlinear Response of Tapered Ceramic Matrix Composite Plates to Base Excitation

S. Michael Spottswood*
U.S. Air Force Research Laboratory, Wright–Patterson Air Force Base, Ohio 45433
and
Marc P. Mignolet†
Arizona State University, Tempe, Arizona 85287

Introduction

THE purpose of this investigation was to study the geometric nonlinear response of tapered ceramic matrix composite (CMC) panels to narrowband random loading at several excitation levels. For each loading scenario, the total strain, or combination of bending and axial strain, was recorded at multiple locations along with the axial and bending strain in the panel center. Results of the study will be used to aid in the development of analytical response and fatigue life prediction tools. A second part of this investigation will be dedicated to the failure mode identification of the panels under extreme acoustic and thermal excitation.

The particular CMC material selected has the potential to be used in structurally integrated thermal protection system applications on future hypersonic, transatomospheric, and reusable space vehicles. CMCs represent a class of materials capable of withstanding the intense thermal and acoustic environments such vehicles would experience. This particular CMC is proposed for structures experiencing temperatures in the 871°C (1600°F) range but is representative of room temperature response and failure of brittle matrix composites.

Blevins et al.[1] and Vaicaitis[2] describe the need for new and exotic materials. They note that even unconventional nickel and iron-based superalloys are limited to 982°C (1800°F) before the onset of oxidation and creep. A transatmospheric vehicle will experience the greatest thermal loading in the nose, engine inlet, and nozzle sections with estimated temperatures exceeding 1650°C (3000°F). Furthermore, acoustic loading due to engine noise alone will exceed 170 dB (Ref. 1). This underscores the need for durable composite materials that can withstand these extreme environments. Nonlinear random vibration testing has been accomplished and described in the literature on metallic structures[3–9] and composite materials,[9–12] but further investigations are necessary due to the complex and often unpredictable behavior of composite structures, particularly for unusual geometries such as the asymmetric tapered panel considered here.

Experimental Procedure

This investigation was conducted in the dynamics and acoustics research facility at Wright–Patterson Air Force Base, Ohio. The panels were manufactured from woven nitrided Nextel 312™/Blackglas™ CMC material and were tapered with the minimum thickness in the panel center to reduce the influence of the boundary conditions on the panel failure mode. Figure 1 shows the dimensions of the CMC panel. The panel was a quasi-isotropic layup of 16 plies $(0/90/45/-45/-45/0/90/45)_S$ around the perimeter panel/clamp interface, reduced to 8 plies $(0/45/-45/90)_S$ in the

Received 23 August 2001; revision received 18 March 2002; accepted for publication 18 March 2002; presented as Paper 2002-372 at the AIAA/ASME/ASCE/AHS/ASC 43rd Structures, Structural Dynamics, and Materials Conference, Denver, CO, 22–25 April 2002. This material is declared a work of the U.S. Government and is not subject to copyright protection in the United States. Copies of this paper may be made for personal or internal use, on condition that the copier pay the $10.00 per-copy fee to the Copyright Clearance Center, Inc., 222 Rosewood Drive, Danvers, MA 01923; include the code 0001-1452/02 $10.00 in correspondence with the CCC.

*Aerospace Engineer, Air Vehicles Directorate. Member AIAA.
†Professor, Department of Mechanical and Aerospace Engineering.

panel center, and was manufactured according to the U.S. Air Force composite ply-drop design guidelines. The taper was accomplished in four steps, with each step reducing the total number of plies by two. Initial analysis and the experimental investigation indicated that the maximum strains occurred in the panel center, even with the experimental clamped boundary conditions.

Critical damping was measured using a PCB Piezotronics, Inc., impulse force hammer and a Polytec, Inc., optical scanning laser vibrometer and vibrometer controller. Measurements were taken with both the scanning laser vibrometer and the impulse force hammer at two separate locations. Results of the damping investigation indicate a critical damping ratio of 2.2% for the fundamental (1,1) panel mode, 310.5 Hz; 0.27% for the (2,1) mode, 385.4 Hz; and 0.39% for the (3,1) mode, 549.1 Hz.

The excitation source and associated equipment utilized for the study was an Unholtz-Dickie Company 53.3-kN (12,000-lbf) electrodynamic shaker, Spectral-Dynamics, Inc., signal generator, and a Measurements Group, Inc., transducer signal conditioner. The base excitation response signal was monitored using a Vibra-Metrics, Inc., Model 1000-A piezoelectric accelerometer, and the panel response was measured using nine Measurements Group, Inc., WK-00-125AD-350 strain gauges, bonded with M-Bond 610 epoxy (Measurements Group, Inc.). The strain gauge locations are also shown in Fig. 1. Because the intent of the investigation was to detect and record the nonlinear strain response in the center of the panel, strain gauges 1 and 2 were attached back-to-back to measure the in-plane or axial, bending, and total strain. This was accomplished through changes in the strain gauge bridge circuitry. The separation of axial and bending strain components assumes that the back-to-back gauges are attached symmetrically. If not, an apparent axial strain could be recorded, resulting in an incorrect bending strain reading as well. Maximum strain occurred in the direction of gauges 1 and 2 in the panel center. A sampling rate of 10 kHz was used throughout the experiment, with the panel natural frequencies of interest significantly less than the Nyquist frequency (see Refs. 4 and 13).

The panel was clamped to the shaker using a steel L-angle fixture and a 32-mm- (1.25-in.-) wide "picture-frame" clamp around the perimeter of the CMC panel to make the test fixture as rigid as possible. This was accomplished for several reasons. First, clamped boundary conditions allow for more straightforward comparisons to analytical work, although in reality the actual experimental boundary conditions are more "relaxed" than theoretical clamped boundary conditions. Second, the experimental rigid boundary conditions did not allow for in-plane expansion, thereby exacerbating the axial stretching, creating the most severe stress field possible.

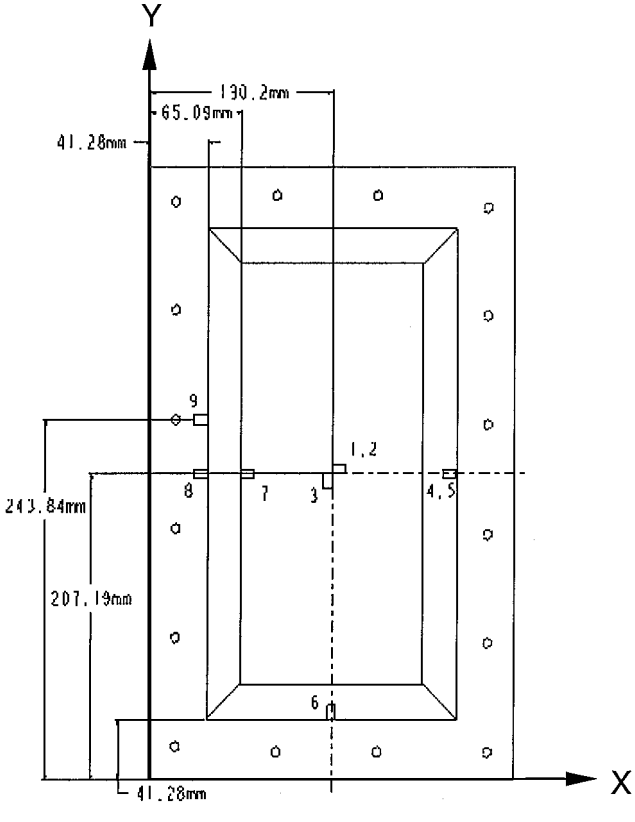

Fig. 1 Strain gauge locations; gauges 2 and 5 located on reverse side of panel.

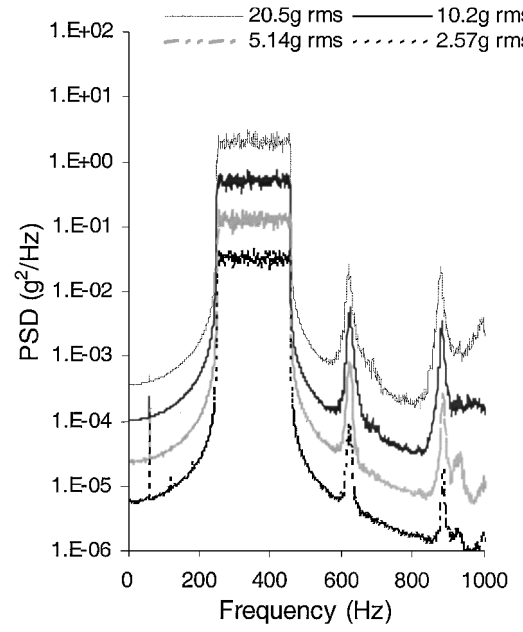

Fig. 2 Narrowband acceleration input spectrum.

The excitation used in the investigation was a narrowband random flat excitation between 250 and 450 Hz, with load levels including 2.57-, 5.15-, 10.2-, and 20.5-g rms (Fig. 2). The narrowband random loading primarily excited the first mode. Note the panel–shaker armature coupling seen as the response at the second harmonic of the panel's fundamental frequency, that is, approximately 620 Hz, and also at 850 Hz in the random loading power spectral densities (PSDs) of Fig. 2. In all instances, the response resulting from the coupling was several orders of magnitude less than the desired excitation levels. The narrowband random loading scenarios provided Gaussian excitation over the prescribed bandwidth, and all loading scenarios were considered stationary after evaluating the mean square response over time.[4]

Experimental Results

The narrowband study was performed at 6-dB increments at the four excitation levels, 20.5-, 10.2-, 5.14-, and 2.57-g rms, with a flat spectrum, between 250 and 450 Hz. The largest total strain rms value was found to be 482 microstrain ($\mu\varepsilon$). Again, the strain time histories were assumed stationary to characterize the PSDs as representative of the entire load history. The total, axial, and bending strain power spectra, in terms of their respective rms strain values for gauge 1, are shown in Figs. 3–5. Again, the panel–shaker coupling effect is noted in Figs. 3–5. The narrowband loading primarily excited the panel fundamental frequency at 310 Hz, as shown in Figs. 3 and 4, therefore dominating the total and bending strain response.

Note the broadening and shifting of the peaks for the total, axial, and bending strain spectra, particularly for the 20.5-g rms excitation case seen in Figs. 3–5.[4,14] This effect is particularly large in the second harmonic peak at 620-Hz. In this context, note, finally, that the two peaks at 310 and 385 Hz in the axial strain PSD have almost merged into a particularly broad peak at the highest excitation level, thereby indicating a change in the qualitative behavior of the axial strains and a strong nonlinear effect. A notable difference is the presence and strength of the 600–620-Hz peak in the different spectra even at low excitation levels. This effect is, however, in part

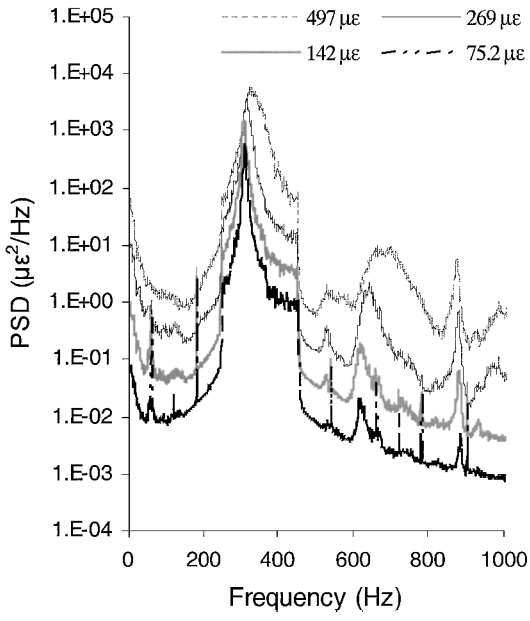

Fig. 3 Spectra of the total strain response to narrowband excitation.

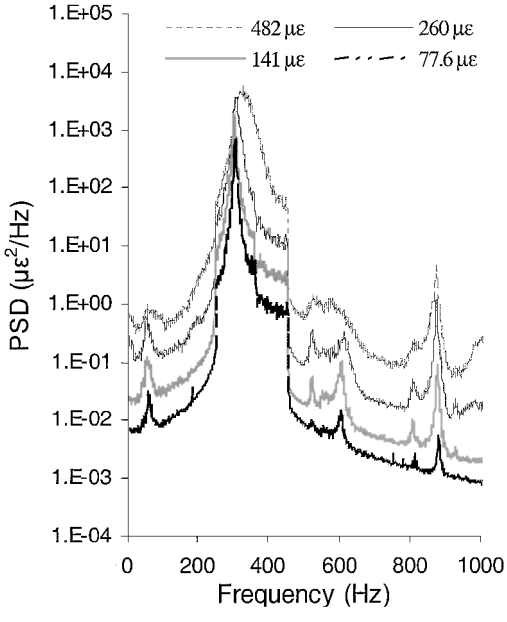

Fig. 4 Spectra of the bending strain response to narrowband excitation.

due to the second harmonic of the 310-Hz fundamental but also to a local peak in the shaker excitation (Fig. 2).

In Fig. 5, note the spike in the axial strain spectra at zero frequency. This is indicative of a nonzero mean, which is readily apparent in Fig. 6, a 1-s representative total, bending, and axial strain time history from the 20.5-g rms broadband excitation scenario. Note that the bending time history of Fig. 6b is relatively symmetric about zero strain, whereas in Fig. 6c, the representative axial strain time history exhibits a nonzero mean, thus resulting in the already mentioned peak in the axial strain power spectra at zero frequency. Note, moreover, in Fig. 6c, the few negative strain excursions in the axial strain time history. Before testing, the panel was found to exhibit a slight curvature resulting from the taper and panel manufacturing process. When the panel was installed in the test fixture, this curvature produced a compressive preload leading to the observed negative values in the axial strain time history.

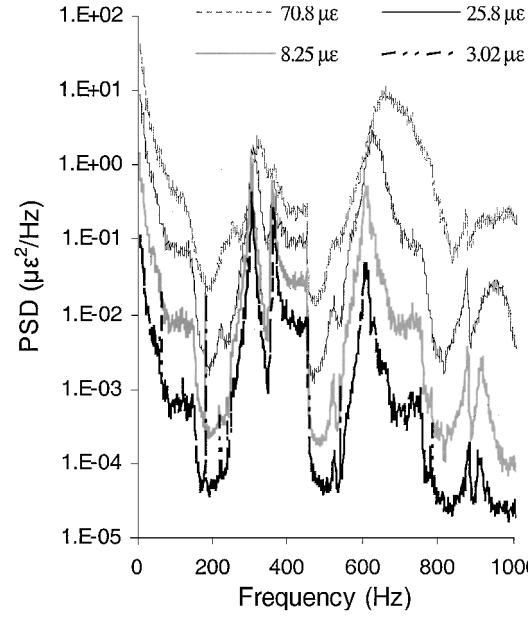

Fig. 5 Spectra of the axial strain response to narrowband excitation.

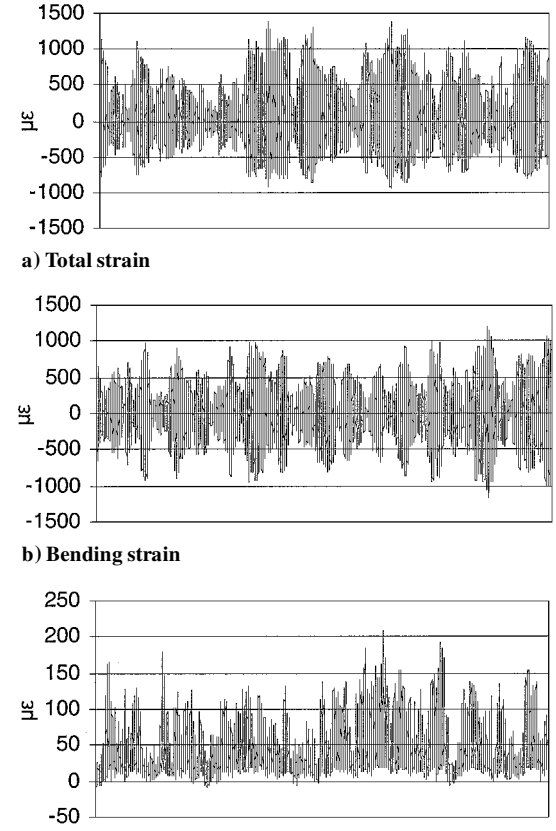

Fig. 6 Time history of 1 s for 20.5-g rms narrowband excitation.

Another point of interest is the effect of the panel taper on the power spectra results. The taper resulted in a condition of asymmetry through the panel thickness even though the composite layup was symmetric. From lamina plate theory, the laminate constitutive equations relating the resultant forces and moments to the strain expressions are

$$\begin{Bmatrix} N \\ M \end{Bmatrix} = \begin{bmatrix} A & B \\ B & D \end{bmatrix} \begin{Bmatrix} \varepsilon^0 \\ \kappa \end{Bmatrix} \tag{1}$$

where $[A]$, $[B]$, and $[D]$ are the elastic in-plane, extension–bending, and flexural rigidity stiffness matrices, respectively. This panel asymmetry resulted in a nonzero $[B]$ matrix and the coupling of the axial, ε^0, and bending, κ, deformations. In a perfectly symmetric panel, the bending strains would be linearly related to the plate transverse displacements, whereas the axial strains would involve the square of the displacements, as shown in the following von Kármán large deflection strain–displacement relations:

$$\{\varepsilon\} = \begin{Bmatrix} \varepsilon_x \\ \varepsilon_y \\ \gamma_{xy} \end{Bmatrix} = \{\varepsilon_m^0\} + \{\varepsilon_\theta^0\} + z\{\kappa\} = \begin{Bmatrix} u_{,x} \\ v_{,y} \\ u_{,y} + v_{,x} \end{Bmatrix} + \frac{1}{2}\begin{Bmatrix} w_{,x}^2 \\ w_{,y}^2 \\ 2w_{,x}\, w_{,y} \end{Bmatrix} + z\begin{Bmatrix} -w_{,xx} \\ -w_{,yy} \\ -2w_{,xy} \end{Bmatrix} \tag{2}$$

where u, v, and w are the displacements along the x, y, and z axes, respectively (Fig. 1), the subscripts m and θ denote the in-plane and large displacement components of the axial strains, respectively, and z is the transverse displacement coordinate.[15] In addition, one would expect to see the peak axial strain to occur at twice the frequency of its bending counterpart. Indeed, the primary axial strain response does occur at approximately 620 Hz. However, the coupling described induces a component of the axial strain that is proportional to the transverse displacements, which is noticeable here by the strong power spectra response at the fundamental bending frequency, 310 Hz.

Consistent with the preceding discussion, note that the axial strain is dominated by the linear (coupling) effect at low excitation levels, as can be seen from the dominance of the 310- and 385-Hz frequencies. As the excitation level is increased, the quadratic effects become larger, and the magnitude of the second harmonics, for example, 620 Hz, rapidly increases. In addition, the squaring involved in obtaining the axial strains from the displacements widens the peak at 620 Hz in comparison with its 310-Hz counterpart. This effect, at least partially, clarifies the significant broadening noted earlier of the 620 Hz with increasing excitation level. In analyzing the relative magnitudes of the peaks, note the importance of the 385-Hz mode at low excitation levels in the axial strains but not in the bending strains. Clearly, the (2,1) mode should be minimally excited by the uniform loading applied here, and its small effect is negligible in the larger bending strains but is relatively significant in the smaller axial strains. As the excitation level increases, the relative magnitude of the second mode effects becomes even less important.

Next, consider the behavior of the overall total, bending, and axial strains vs excitation level. Figure 7 shows the respective mean square levels on a logarithmic scale, whereas Fig. 8 shows the mean values on a linear scale. The axial strain contributes little to the mean square total strain response, from 4% at low excitation levels to 14% at the highest one, as shown in Fig. 7. Notice that the mean square of the various strains grows slightly less than linearly with the excitation level. This result could be expected for the bending strains, given their approximate [with $[B]$ of Eq. (1) nonzero] linear dependence with respect to the transverse displacement and the hardening nonlinear character of the panel response. A rather different situation is shown in Fig. 8 for the mean of the strains: At higher levels, the axial strains become preponderant. Furthermore, the mean of the bending strains is approximately linear while the axial strain displays a sharp quadratic relationship with the excitation level. The presence of a nonzero mean bending strain is clearly associated with the asymmetry in the transverse displacements resulting from the taper. The linearity of the mean is a reflection of the approximate linearity of the bending displacements and strains for most of the excitation range. It would be expected that the mean axial strain would also exhibit, at low excitation levels, a linear behavior corresponding to the bending–axial coupling created by the asymmetric taper, which was already responsible for the presence of the 310- and 385-Hz peaks in Fig. 5. This component, however, appears to be quite small because the quadratic effect dominates through most of the excitation level range. It is clear from Fig. 8 that the asymmetry of the total strains is almost exclusively due to the axial component, although the asymmetry of the bending strains is also, but more slowly, increasing.

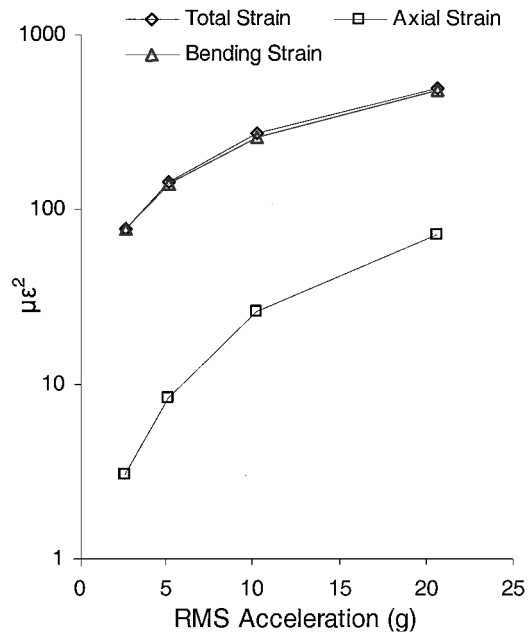

Fig. 7 Mean square strain of gauge 1 in the panel center, perpendicular to and in the direction of the longest edge, narrowband excitation.

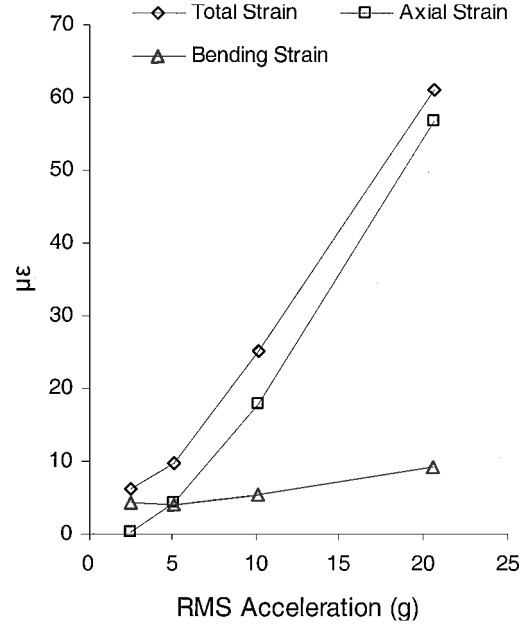

Fig. 8 Mean strain of gauge 1 in the panel center, perpendicular to and in the direction of the longest edge, narrowband excitation.

The final discussion of the narrowband loading results will focus on the corresponding strain rainflow, peak, and amplitude response distributions of Figs. 9–11. Figures 10 and 11 are scaled with their respective standard deviations. The rainflow cycle counting technique seeks to match a local maximum peak with a local minimum valley in the time record, forming a strain hysterisis loop where the strain range is defined as the difference between the local peak and valley. The American Society for Testing and Materials algorithm was used for this investigation (see Refs. 16 and 17). As expected, the nonlinear effects manifested themselves in the probability density functions (PDFs). Consider first the PDF of the scaled rainflow strain ranges (Fig. 9) displayed in terms of the respective total rms strain values. While regressing approximately to a common distribution, there is a noticeable shift to the right as the excitation

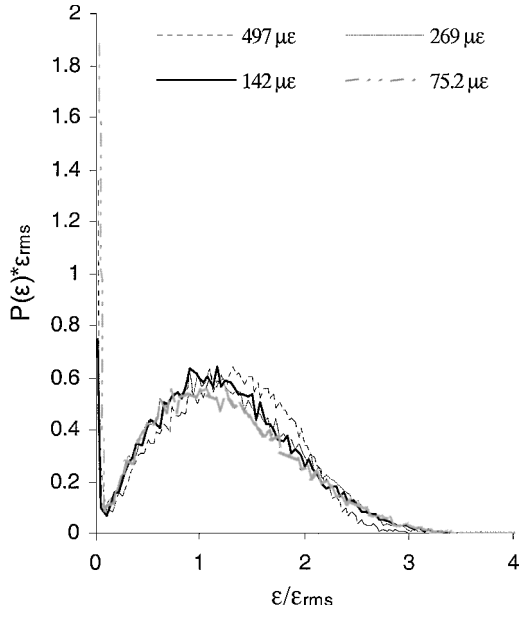

Fig. 9 Total strain rainflow PDF of strain gauge 1, narrowband excitation.

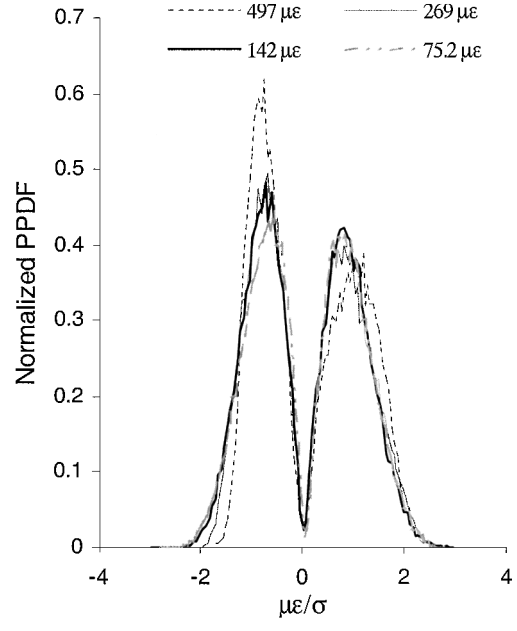

Fig. 10 Total strain peak PDF of strain gauge 1, narrowband excitation.

level increases. The direction of the shift may seem counterintuitive at first. Indeed, because the nonlinearity is of a hardening type, the peak amplitudes grow slower than linear amplitudes, and, thus, proportionally smaller ranges would be expected as the excitation level is increased. This scenario is indeed appropriate for the transverse displacements, but the linear and square terms involved in the displacement–strain relation lead to a nonuniform stretching of the displacements into strains. This transformation affects the large positive displacements more than the small ones and, thus, provokes the shift of the positive peak values to levels higher than would be seen from a linear model (Fig. 10).

A reverse effect, but of lesser magnitude, is obtained for the negative displacements; see the shift of the compressive strains in Fig. 10. The overall effect of this transformation is, thus, an increase of the cycle amplitudes as seen in Fig. 9 and the prominent asymmetry of the total strain peak PDF in Fig. 10, which increases with the

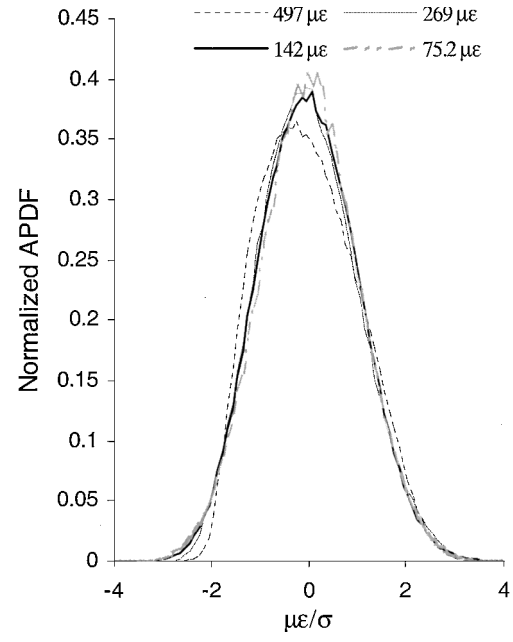

Fig. 11 Total strain PDF of strain gauge 1, narrowband excitation.

excitation level. This observation is in agreement with Lee[18] and Steinwolf and White.[19] To maintain the total probability to one, the normalized compressive strain peak must increase in magnitude as it narrows with increasing excitation level. On the contrary, the normalized tensile strain peak both reduces and widens. This behavior is the result of the growing significance of the axial strains, which directly relate to the quadratic component of the displacement–strain relation. In this regard, note that the mean value of the axial strains is a more direct quantifier of the quadratic term and its peak shifting effects than the mean square axial strains.

Finally, examining the amplitude PDF of Fig. 11, a tendency toward asymmetry is also noticed. As discussed earlier, both the number of smaller amplitude compressive excursions and the number of larger amplitude tensile excursions increase with increasing excitation level, thereby increasing the tendency of the strain PDF to lean to the left, or a display of non-Gaussian behavior.

Conclusions

The geometric nonlinear response of a tapered, clamped CMC panel to narrowband Gaussian random excitations has been investigated. The panels were manufactured according to U.S. Air Force ply-drop guidelines, characteristic of future aircraft structures and materials. With renewed emphasis on space and hypersonic vehicles, the panel material is of interest to the U.S. Air Force. The characteristics of the excitation response PSDs, sample time-histories, mean and mean square relationships to excitation, and the PDFs were studied. Of particular interest were the effects of the coupling between the bending and axial strain response, resulting from the through-the-thickness asymmetry of the panel taper. The result of the asymmetry was noticeable in the axial strain PSDs shown in Fig. 5, at all excitation levels. In particular, at low excitation levels, the axial strain PSD exhibited sharp peaks at the primarily bending natural frequencies of the panel. In fact, at all excitation levels, the panel response at the fundamental frequency, 310 Hz, continued to play a dominant role. The taper asymmetry was also clearly visible from the mean strains. Finally, the narrowband excitation loading scenarios resulted in a geometric nonlinear response, as evidenced by the peak shifting and broadening effects in the strain response PSDs, and also by an axial strain effect, or the noted asymmetry and/or peak shifting in the narrowband PDFs.

Acknowledgments

This research was sponsored by the Air Force Office of Scientific Research as part of the Air Force New World VISTA research

program. The authors would like to thank Dansen Brown, U.S. Air Force Research Laboratory/VASS, for his invaluable assistance in data analysis. Also, the authors gratefully acknowledge the assistance and expertise of Larry Simmons, the Structural Dynamics and Acoustics Branch facility technician.

References

[1]Blevins, R. D., Holehouse, I., and Wentz, K. R., "Thermoacoustic Loads and Fatigue of Hypersonic Vehicle Skin Panels," *Journal of Aircraft*, Vol. 30, No. 6, 1993, pp. 971–978.

[2]Vaicaitis, R., "Nonlinear Response and Sonic Fatigue of National Aerospace Plane Surface Panels," *Journal of Aircraft*, Vol. 31, No. 1, 1994, pp. 10–18.

[3]Chen, R. R., Mei, C., and Wolfe, H. F., "Comparison of Finite Element Nonlinear Beam Random Response with Experimental Results," *Journal of Sound and Vibration*, Vol. 195, No. 5, 1996, pp. 719–737.

[4]Ibrahim, R. A., "Nonlinear Random Vibration: Experimental Results," *Applied Mechanics Review*, Vol. 44, No. 10, 1991, pp. 423–446.

[5]Wolfe, H. F., Camden, M. P., Wentz, K. R., and Simmons, L. W., "Determining the Peak Probability Distribution Function of the Nonlinear Random Response of a Clamped Plate," *Proceedings of the Second International Conference on Non-Linear Problems in Aviation and Aerospace*, Vol. 2, European Conference Publ., Cambridge, England, U.K., 1999, pp.787–796.

[6]Koenig, K., Gunther, M., and Grahlmann, U., "Some Remarks on the Acoustic Fatigue of Aluminum Structures with either Integrally Milled or Riveted Edge Reinforcements," *Aerospace Science and Technology*, Vol. 2, No. 1, 1998, pp. 27–36.

[7]Ng, C. F., "Nonlinear and Snap-Through Responses of Curved Panels to Intense Acoustic Excitation," *Journal of Aircraft*, Vol. 26, No. 3, 1989, pp. 281–288.

[8]Ng, C. F., and Clevenson, S. A., "High Intensity Acoustic Tests of a Thermally Stressed Plate," *Journal of Aircraft*, Vol. 28, No. 4, 1991, pp. 275–281.

[9]Wolfe, H. F., Shroyer, C. A., Brown, D. L., and Simmons L. W., "An Experimental Investigation of Nonlinear Behavior of Beams and Plates Excited to High Levels of Dynamic Responses," U.S. Air Force Wright Research and Development Center, WL-TR-96-3057 1995 WL/FIBG, Wright–Patterson AFB, OH, Oct. 1996.

[10]Istenes, R. R., Rizzi, S. A., and Wolfe, H. F., "Experimental Nonlinear Random Vibration Results of Thermally Buckled Composite Panels," *Proceedings of the 36th Structures, Structural Dynamics, and Materials Conference*, AIAA, Washington, DC, 1995, pp. 1559–1568.

[11]Wolfe, H. F., Camden, M. P., Byrd, L. W., Paul, D. B., and Simmons, L. W., "Failure Criteria Development for Dynamic High-Cycle Fatigue of Ceramic Matrix Composites," *Journal of Aircraft*, Vol. 37, No. 2, 2000, pp. 319–324.

[12]Wolfe, H. F., Camden, L. W., Paul, D. B., and Simmons, L. W., "Sigma Limiting Effects on the Response of a Ceramic Matrix Beam," AIAA Paper 99-1456, 1999.

[13]Randall, R. B., *Frequency Analysis*, K. Larsen and Søn A/S, Glostrup, Denmark, 1987.

[14]Schudt, J. A., "The Response of Nonlinear Systems to Random Excitation," M.S. Thesis, Dept. of Engineering Mechanics, Ohio State Univ., Columbus, OH, 1991.

[15]Mei, C., Dhainaut, J. M., Duan, B., Spottswood, S. M., and Wolfe, H. F., "Nonlinear Random Response of Composite Panels in an Elevated Thermal Environment," U.S. Air Force Research Lab., AFRL-VA-WP-TR-2000-3049, Wright–Patterson AFB, OH, Oct. 2000.

[16]Anzai, H., "Algorithm of the Rainflow Method," *Proceedings of the International Symposium on Fatigue Damage Measurement and Evaluation under Complex Loading. The Rainflow Method in Fatique—The Tatsuo Endo Memorial Volume*, Fukuoka, Japan, 1991, pp. 11–20.

[17]Bannantine, J. A., Comer, J. J., and Handrock J. L., *Fundamentals of Metal Fatigue Analysis,* Prentice–Hall, Upper Saddle River, NJ, 1990, pp. 193–196.

[18]Lee, J., "Displacement and Strain Statistics of Thermally Buckled Plates," *Journal of Aircraft*, Vol. 38, No. 1, 2001, pp. 104–110.

[19]Steinwolf, A., and White, R. G., "Probability Density Functions of Acoustically Induced Strains in Experiments with Composite Plates," *AIAA Journal*, Vol. 35, No. 12, 1997, pp. 1853–1861.

A. N. Palazotto
Associate Editor

Stability of Spring-Hinged Cantilever Column Under Combined Concentrated and Distributed Loads

G. Venkateswara Rao* and K. Kanaka Raju†
Vikram Sarabhai Space Center, Trivandrum 695 022, India

Nomenclature

a, b	=	undetermined coefficients in Eq. (6)
a_1–a_6	=	functions defined in Eq. (8)
E	=	Young's modulus
I	=	area moment of inertia
k	=	stiffness of the rotational spring
L	=	length of the column
P	=	end-concentrated axial load
P_{cr}	=	critical P
q	=	uniformly distributed axial load
q_{cr}	=	critical q
W	=	lateral displacement distribution
w	=	nondimensional lateral displacement, W/L
α	=	$\lambda_q/\lambda_{q\,\text{cr}}$
α_1–α_3	=	undetermined coefficients in Eq. (2)
β	=	$\lambda_P/\lambda_{p\,\text{cr}}$
γ	=	rotational spring stiffness parameter, kL/EI
λ_p	=	concentrated axial load parameter, PL^2/EI
λ_q	=	uniformly distributed axial load parameter, qL^3/EI
$\lambda_{p\,\text{cr}}$	=	critical λ_p
$\lambda_{q\,\text{cr}}$	=	critical λ_q
ξ	=	nondimensional axial coordinate x, x/L
$'$	=	differentiation with respect to ξ

Introduction

THE upper stage of solid motor rockets and missiles is a highly optimized structure required to be designed to achieve higher payload capability. The fore end of this stage is connected to the payload through a payload adaptor, and the aft end is connected to a relatively stiffer stage through interstage structure that is flexible in rotation. In service condition, the rockets and missiles are subjected to very high axial acceleration. Because of this and the mass of the payload and payload adaptor, the fore end of the upper stage is subjected to a high axial compressive concentrated load. The upper stage is also subjected to a uniformly distributed axial compressive load due to its own inertia. As such, the upper stage can be idealized as a uniform cantilever column simultaneously subjected to an axial compressive concentrated load at the free end and a uniformly distributed axial compressive load along the length of the column, the two loads being mutually independent and acting simultaneously. The aft end of the column, where rotation is allowed, can be modeled as a spring-hinged end because of the rotational flexibility of the interstage structure with the lateral displacement constrained. Thus, the analytical model turns out to be a three-parameter problem, and it is often necessary to obtain the stability behavior of such columns to assess their structural integrity.

Even though the versatile finite element method[1] (FEM) can be effectively used to solve this problem, it becomes laborious and time consuming because of the parametric study involved with three parameters. Hence, development of an accurate closed-form solution

Received 4 April 2001; revision received 14 September 2001; accepted for publication 9 May 2002. Copyright © 2002 by the American Institute of Aeronautics and Astronautics, Inc. All rights reserved. Copies of this paper may be made for personal or internal use, on condition that the copier pay the $10.00 per-copy fee to the Copyright Clearance Center, Inc., 222 Rosewood Drive, Danvers, MA 01923; include the code 0001-1452/02 $10.00 in correspondence with the CCC.

*Scientist/Engineer, Structural Engineering Group; gv_rao@vssc.org.
†Scientist/Engineer, Structural Engineering Group.